AB

CERN LIBRARIES, GENEVA
SCAN-9507027

UB-HEX-95-02

Two- and Three-Particle Correlations in Gold-Emulsion Interactions at 10.6A GeV

A. Mukhopadhyay, P. L. Jain and G. Singh
High Energy Experimental Laboratory
Department of Physics
State University of New York at Buffalo Buffalo, New York 14260

SW9528

April 28, 1995

Abstract

We present an analysis on two- and three-particle correlations among shower particles, produced in semicentral collisions of ^{197}Au at 10.6A GeV with nuclear emulsion. Results are compared with the existing data of ^{28}Si ion at 14.5A GeV from BNL, and ^{32}S, ^{16}O nuclei at 200A GeV and ^{16}O beam at 60A GeV from CERN. Existence of short-range correlations is observed to be a general feature of all the heavy-ion reactions in pseudorapidity and azimuthal angle phase-spaces.

PACS Numbers: 25.70.Np

1 Introduction

The recent interest in heavy-ion collisions prevails in the possibility of creating hadronic systems with high matter density, where one may expect new phenomenon to occur. One of the important topics considered most recently is to search for the non-statistical multiplicity fluctuations in small intervals of pseudorapidity, which may provide a signature of deconfined phase of quark-gluon-plasma leading to intermittent behavior. Bialas and Peschanski [1] have proposed an analysis of the pseudorapidity density distributions in terms of normalized factorial moments to investigate the intermittency. However, it has been cautioned by Carruthers et al. [2] that the intermittency phenomenon could be understood in terms of conventional short-range Bose Einstein correlations, the Hanbury-Brown Twiss (HBT) effect or the Goldhaber (GGL) effect for identical particles [3], and cumulant moments of order greater than two are strongly suppressed. If the higher order cumulant moments suddenly increase, they will reflect the presence of more violent bulk fluctuations preceding the hadronization. Therefore, the study of two- or three-particle correlation functions in heavy-ion experiments needs a careful and systematic exploration.

Correlations are known to contain trivial backgrounds. For example, the two-particle rapidity density $\rho^{(2)}(y_1, y_2)$ factorizes into components $\rho^{(1)}(y_1)\rho^{(1)}(y_2)$ when two variables y_1, y_2 become statistically independent. True statistical correlations are, therefore, obtained only after filtering out such trivial contributions. A two-particle correlation function [4] is defined as:

$$C_2(y_1, y_2) = \rho^{(2)}(y_1, y_2) - \rho^{(1)}(y_1)\rho^{(1)}(y_2), \quad (1)$$

where $\rho^{(2)}(y_1, y_2) = \sigma_{in}^{-1} d^2\sigma/dy_1 dy_2$ and

Appearing in Nuovo Cim. A (1995)

$\rho^{(1)}(y) = \sigma_{in}^{-1} d\sigma/dy$ are, respectively, the two- and one-particle rapidity densities of produced particles, and σ_{in} is the total inelastic cross-section; $d^2\sigma/dy_1 dy_2$ and $d\sigma/dy$ are, respectively, the two- and one-particle semi-inclusive distributions. It is often more advantageous to use a normalized correlation function,

$$R_2(y_1, y_2) = C_2(y_1, y_2)/\rho^{(1)}(y_1)\rho^{(1)}(y_2), \quad (2)$$

which is less sensitive to experimental errors than $C_2(y_1, y_2)$. The correlation function $R_2(y_1, y_2)$ is related to the density of emitting sources [5]. The three-particle correlation function is also defined in a similar way:

$$\begin{aligned} C_3(y_1, y_2, y_3) &= \rho^{(3)}(y_1, y_2, y_3) \\ &- \rho^{(1)}(y_1)\rho^{(2)}(y_2, y_3) - \rho^{(1)}(y_2)\rho^{(2)}(y_3, y_1) \\ &- \rho^{(1)}(y_3)\rho^{(2)}(y_1, y_2) \\ &+ 2\rho^{(1)}(y_1)\rho^{(1)}(y_2)\rho^{(1)}(y_3), \end{aligned} \quad (3)$$

while the normalized three-particle correlation function is,

$$\begin{aligned} &R_3(y_1, y_2, y_3) = \\ &C_3(y_1, y_2, y_3)/\rho^{(1)}(y_1)\rho^{(1)}(y_2)\rho^{(1)}(y_3). \end{aligned} \quad (4)$$

Here, $\rho^{(3)}(y_1, y_2, y_3) = \sigma_{in}^{-1} d^3\sigma/dy_1 dy_2 dy_3$ is the three-particle rapidity density, and $d^3\sigma/dy_1 dy_2 dy_3$ is the three-particle semi-inclusive distribution.

With the advent of factorial moments as a topic of investigation, it has recently been pointed out that the normalized factorial moments and factorial correlators are the integrals of the same underlying correlation function, and are very closely related to the above mentioned C_q's ($q = 2, 3$) [2]. A great deal of attention has been paid on measuring normalized factorial moments [6], and thus, the importance of analyzing the data in terms of different C_q functions is undeniable. The present work involves computing two- and three-particle correlations, in pseudorapidity (η) and azimuthal angle (ϕ) phase spaces, of shower particles produced in ^{197}Au-emulsion collisions at 10.6A GeV (beam A) from the Alternating Gradient Synchrotron (AGS) at Brookhaven National Laboratory (BNL). We also compare the results of beam A with the available data from our Laboratory of four additional data samples [7]: (i) ^{28}Si at 14.5A GeV (beam B), (ii) ^{32}S at 200A GeV (beam C), (iii) ^{16}O at 200A GeV (beam D) and (iv) ^{16}O at 60A GeV (beam E).

The paper is organized as follows. In Section 2, we discuss the experimental technique. Section 3 is devoted to the results and their discussions on two-particle and three-particle correlations in η as well as in ϕ phase-spaces. Finally, the conclusions of this work are presented in Section 4.

2 Experimental Technique

In this investigation, we have used the data obtained from a recent experiment performed at the BNL (Expt. No. 875) with a newly extracted beam of ^{197}Au ions at 10.6A GeV (beam A). Further details of the experiment, scanning and selection of events can be found in Ref. [8]. For the present report, we employed a sample of semicentral events with at least with 50 produced shower tracks, N_s and also the charges of the projectile fragments (PF's) were confined in the range $1 \leq Z \leq 17$. Out of a data set of about 1500 along-the-track scanned inelastic interactions, 245 events were retained for the current study. Angular measurements of all the tracks emerged in 245 collisions were made by using relative primary method [9], and thus, resulting an accuracy of 0.1 mrad for the very forward proceeding tracks. For beam B, the data were obtained from an Experiment No. 847 performed at the BNL, while for projectiles C, D and

E, we used the data of Experiment No. EMU08 conducted at the CERN SPS. The details of data acquisition procedures, event selection criteria, and angle measurement techniques for ions B, C, D and E are described in our earlier reports [7,9]. For the beams B, C, D and E, only central events, with complete destruction of the projectile nucleus into singly charged protons tracks, are considered. The number of such events used for B, C, D and E projectiles is 172, 200, 280 and 179, respectively. Average number of produced shower particles $< N_s >$ in these collisions is: (A) 181 ± 12, (B) 73 ± 6, (C) 216 ± 15, (D) 119 ± 7 and (E) 81 ± 6. The shower particles are mostly produced charged mesons having relativistic velocities ($v > 0.7c$). Pseudorapidity [$\eta = -\ln\tan(\theta/2)$] is oftenly employed to locate a particle in η phase-space, where θ is the emission angle of a given particle. In nuclear emulsion, it is difficult to make a definite distinction between singly charged produced particles, and a projectile fragment of the same charge. The projectile fragments are emitted, in general, within a narrow forward cone of semivertex angle θ_c [$\theta_c = 0.2/p_{beam}$, and p_{beam} (GeV/c) is the incident beam momentum per nucleon]. We eliminated all the particles falling into this cone from the present analysis.

The determination of experimental values of two- or three-particle correlation functions ultimately involves counting of shower particles at a particular η value, or more specifically within a very narrow η-bin around that η. For this purpose, we express the normalized correlation functions into more convenient forms as:

$$R_2(\eta_1,\eta_2) = \frac{N_T\,N_2(\eta_1,\eta_2)}{N_1(\eta_1)N_1(\eta_2)} - 1, \qquad (5)$$

and,

$$R_3(\eta_1,\eta_2,\eta_3) = \frac{N_T^2 N_3(\eta_1,\eta_2,\eta_3)}{N_1(\eta_1)N_1(\eta_2)N_1(\eta_3)} - \frac{N_T N_2(\eta_1,\eta_2)}{N_1(\eta_1)N_1(\eta_2)} - \frac{N_T N_2(\eta_2,\eta_3)}{N_1(\eta_2)N_1(\eta_3)} - \frac{N_T N_2(\eta_3,\eta_1)}{N_1(\eta_3)N_1(\eta_1)} + 2. \qquad (6)$$

Here, N_T is total number of inelastic events used after the applied cuts; $N_1(\eta)$ is number of shower particles at η; $N_2(\eta_1,\eta_2)$ is the number of pairs of shower particles at η_1 and η_2; $N_3(\eta_1,\eta_2,\eta_3)$ is the number of triplets of shower particles at η_1, η_2 and η_3. A similar analysis is also valid for the azimuthal angle phase-space, ϕ.

It is worthwhile to mention, that we have confined our analysis mainly in the pionization region of pseudorapidity phase-space for the projectiles A, B, C, D and E. For the ions A and B obtained from the BNL, the chosen $\Delta\eta = \eta_2 - \eta_1$ interval was 1.0-4.0, while for the CERN projectiles C, D and E, this range was 1.0-6.5 units in η phase-space. In ϕ phase-space, the analysis was restricted only to those shower tracks which fell in the above mentioned $\Delta\eta$ ranges of beams A, B, C, D and E.

3 Results and discussion

3.1 *Two-particle correlations in η phase-space*

For a specific type of interaction, when we examine the values of $R_2(\eta_1,\eta_2)$ for a particular η_1 and at different η_2, we often find maxima at $\eta_2 \approx \eta_1$ [10]. The peak value of $R_2(\eta_1,\eta_2)$ is > 0, and it decreases as η_2 shifts away from η_1. This feature being common in high energy hadronic or nuclear reactions [10]; no schematic representation of the data is given in this regard. Instead, we have plotted the $R_2(\eta_1,\eta_2)$ against η at equal pseudorapidities, e.g., $\eta_2 = \eta_1$, for two different projectiles A and B obtained from the BNL in Fig. 1(a), while for the CERN projectiles C, D and E, a similar plot is presented in Fig. 1(b). Each data point in such a plot is a measure of short-range two-particle correlation at a particular region of η phase-space. The

error bars on the data points were always negligible, and hence are not shown in Figs. 1(a) and 1(b). Another common aspect of our data, as seen from Figs. 1(a) and 1(b) is that, the R_2 value at equal η, declines with increasing η (to their projectile rapidities η_{proj}) for all the reactions studied. As a consequence, projectiles C and D with the highest energy per nucleon have longer tails as compared to the low energy data of A, B and E beams. The general feature of the results obtained from above analysis is the existence of two-particle short-range correlation in all the heavy-ion interactions of projectiles A, B, C, D and E accelerated at relativistic energies.

The structure of such semi-inclusive correlations observed in Fig. 1 may arise from mixing of events with different impact parameters in pseudorapidity phase-space, and so, it may not reflect the true correlation. Therefore, studying correlations for a certain category of events by fixing the multiplicity of shower particles N_s is oftenly suggested. To achieve this goal, we splitted each of the data sets into three subgroups depending upon the multiplicities of shower particles in such a way that the statistics of these subsets are quite reasonable. For each subgroup of events for an individual projectile, the values of R_2 were computed separately. Among all the data sets, beams A and C of heavier masses have the highest average multiplicities of shower particles. We chose the following the criteria to divide their multiplicity into three subgroups: $N_s \leq 150$ (A1, C1), $150 < N_s \leq 250$ (A2, C2) and $N_s > 250$ (A3, C3), and the statistics of events for these subgroups are: 111, 52; 81, 74; and 53, 74; with average shower particle multiplicities: 110 ± 10, 109 ± 15; 195 ± 22, 195 ± 23, and 300 ± 41, 313 ± 36; respectively. It is interesting to note that average multiplicity of shower particles in these subgroups for the beams A and C is almost the same. The normalized two-particle correlation functions $R_2(\eta_1, \eta_2)$ are computed from Eq. (5) for the three multiplicity subgroups, and are shown in Figs. 2(a), 2(b), 2(c) for ion A, and in Figs. 2(d), 2(e), 2(f) for beam C, where we plot $R_2(\eta_1, \eta_2)$ vs. η at $\eta_1 = \eta_2$. The error bars associated with each data point is only of statistical origin [11]. For ion A in subgroups A1 and A2, two-particle correlation function $R_2(\eta_1, \eta_2)$ declines as a function of η, while in subgroup A3, it stays almost constant. Among the subgroups $A1$, $A2$ and $A3$, the magnitude of the correlation function is the largest in A3 subgroup, which may be due to the effect of resonances present among the produced particles in the central collisions. For beam C in subgroup C1, R_2 decreases as a function of η just like in subgroups A1 and A2 of beam A. In subgroups C2 and C3, except for the last data point, the correlation function R_2 remains almost saturated within the error bars for each beam. But, the values of R_2 for a heavier ^{197}Au ion in subgroup A_3 are a factor of two higher than a lighter ^{32}S ion in subset C_3 throughout the entire range of η. None of the subgroups of beams A and C shows any peculiar behavior in two-particles correlation in η phase-space. Similar results were also obtained for ions B, D and E, and no attempt has been made to present them graphically in this study. Thus, all the data samples with quite different beam mass and energy do not possess any unusual two-particle correlation in η phase-space on the basis of three different multiplicity subdivisions.

3.2 *Three-particle correlations in η phase-space*

We now proceed to compute the three-particle correlations using Eq. (6). In Fig. 3(a), we have plotted the normalized three-particle correlation functions $R_3(\eta_1, \eta_2, \eta_3)$ at equal intervals of pseudorapidities ($\eta_1 = \eta_2 = \eta_3$) against η for the projectiles A and B obtained from the BNL. Three-particle correlation function R_3 is little higher for beam A as compared to ion B. Other data sets of projectiles C, D and E pre-

sented in Fig. 3(b) also show the existence of some positive correlations. The correlation function R_3 for ions C and E exhibits almost a similar behavior except for the last two or three data points, whereas for beam D, it declines with an enhancement in η. In Figs. 3(a) and 3(b), the errors bars are negligible and are not shown here.

To study the impact parameter dependence of three-particle correlation function R_3 in η phase-space, we again employ the same multiplicity cuts on the number of shower particles N_s as was done in Fig. 2 for ions A and C. For subsets A1, A2 and A3, the results are depicted in Figs. 4(a), 4(b) and 4(c), respectively. Subsets A1 and A2 show a decline in R_3 from an initial maximum value to a final minimum value, when η is enhanced from 1.0 to 4.0, while for the subgroup A3, R_3 remains constant within the error bars. However, R_3 vlaues for group A_3 are much higher than for groups A_1 and A_2. This may be due the presence of resonances among the produced particles in the most violent collisions with $N_s > 250$. Similar characteristics were also revealed for two-particle correlation function R_2 for beam A in η phase space. For beam C, we now plot three-particle correlation function R_3 vs. η in Figs. 4(d), 4(e) and 4(f) on the basis of respective multiplicity subgroups C1, C2 and C3. In each of the three subgroups, some positive and finite correlation strength is observed. Among these three subsets, subset C1 possesses the maximum three-particle correlation strength R_3. The behavior of beam A is different from that of ion C in each of the subsets. However, a gross feature of positive and finite three-particle correlation function is clearly obvious for the data sets of beams A and C in three different multiplicity cuts. Similar observations were also made for projectiles B, D and E (not shown here).

3.3 *Two- and three-particle correlations in ϕ phase-space*

It is interesting to explore the nature of two-particle correlation function $R_2(\phi_1, \phi_2)$ against ϕ at equal bins of azimuthal angles, $\phi_2 = \phi_1$, for all the ions used in the present study. First, we turn to our results on two different projectiles A and B obtained from the BNL. This is shown in Fig. 5(a). The error bars were always negligible, and hence, are not plotted in this figure. At all values of ϕ, positive two-particle correlations $R_2(\phi_1, \phi_2)$ are clearly seen for the ions accelerated at the BNL AGS. The ^{197}Au data at 10.6A GeV show higher correlation than the ^{28}Si data set at each value of ϕ. For ^{197}Au beam, correlation is relatively stronger at $\phi \approx 90^0$ and $\phi \approx 270^0$ as reported earlier [12]. Data for beams C, D and E obtained from the CERN SPS are presented in Fig. 5(b). We may notice that the ions C and E have almost the same strength of two-particle correlation function $R_2(\phi_1, \phi_2)$, whereas the ion D has higher magnitude of $R_2(\phi_1, \phi_2)$, especially at $\phi \approx 90^0$ and $\phi \approx 270^0$, in comparison to the beams C and E. In Fig. 6, we present the data of two-particle correlation function R_2 in ϕ phase-space for ^{197}Au and ^{32}S ions with $N_s > 250$: the extremely central interactions among all the data sets used. Both data sets exhibit a constant behavior for different vlaues of ϕ, except for $\phi \approx 270^0$ of the ^{32}S data. The magnitude of the correlation function R_2 for ^{197}Au beam is much higher than that of ^{32}S data: it may be an effect of heavier mass.

We repeated the three-particle correlation function R_3 calculations in azimuthal angle phase-space to examine their structures for projectiles A, B, C, D and E as was done in Section 3.2. The three-particle correlation function $R_3(\phi_1, \phi_2, \phi_3)$ against ϕ at equal bins of azimuthal angles, $\phi_1 = \phi_2 = \phi_3$, is displayed in Fig. 7(a) for beams A and B. In general, the magnitude of $R_3(\phi_1, \phi_2, \phi_3) < R_2(\phi_1, \phi_2)$ for

all the samples employed in the current study. As in case of two-particle correlation function $R_2(\phi_1, \phi_2)$, the three-particle correlation function $R_3(\phi_1, \phi_2, \phi_3)$ at each value of ϕ has also higher correlation strength for ion A than that of beam B, and especially at $\phi \approx 90^0$ and $\approx 270^0$. Results of three-particle correlation of ions C, D and E are presented in Fig. 7(b). Once again, some positive and finite three-particle correlations are observed for all the CERN SPS ions in ϕ phase-space, while for beam D, R_3 values are higher at $\phi \approx 90^0$ and $\approx 270^0$ just like in R_2 values for this beam(D). We now perform the three-particle correlation analysis for the most central events of ^{197}Au and ^{32}S having $N_s > 250$ in ϕ phase-space. Results of this analysis are presented in Fig. 8. Just like in Fig. 6, both the subgroups show almost a constant behavior of $R_3(\phi_1, \phi_2, \phi_3)$, for different values of ϕ, except for a few data pionts for the subset C_3 of ^{32}S beam at $\phi \approx 270^0$. Once again, the magnitude of the correaltion function R_3 is much higher for the massive ^{197}Au projectile accelerated from the BNL AGS.

4 Conclusions

From the observations made in the present investigation, we conclude that short-range two and three-particle correlations exist among the shower particles produced in relativistic heavy-ion collisions of all the projectiles A, B, C, D and E used in the current study. In η as well as ϕ phase-space, two- or three-particle correlation strength (R_2 or R_3), in general, seems to be higher for heavier ion ^{197}Au at 10.6A GeV as compared to ^{28}Si ion at 14.5A GeV. It may be the effect of collective flow in heavier masses. By subdividing the data sets of ^{197}Au ion at 10.6A GeV from the BNL AGS and of ^{32}S beam at 200A GeV from the CERN SPS on the basis of three different multiplicity cuts at three different impact parameters, in η as well as in ϕ phase-spaces, the correlation functions R_2 and R_3 are stronger for the most central events with $N_s > 250$ of ^{197}Au ion as compared to ^{32}S ion. The observed correlations may be due to the decay of resonances, Bose-Einstein correlations or the effect of residues of HBT type correlations in the ^{197}Au data obtained from BNL. Two- and three-particle short-range correlation is found to be an intrinsic characteristic of all the heavy-ion reactions studied in the present experiment.

Acknowledgements

We are thankful to Prof. G. Vanderhaeghe, the technical staff of CERN, Dr. D. Beavis, BNL for their help in the exposure, and to Prof. G. Romano for the development of our emulsion stacks. This research work is supported partially by the Research Foundation of State University of New York at Buffalo.

References

[1] A. Bialas and R. Peschanski, Nucl. Phys. B **273**, 703 (1986).

[2] P. Carruthers, H. C. Eggers and I. Sarcevic, Phys. Rev. C **44**, 1629 (1991).

[3] R. Hanbury-Brown, R. Q. Twiss, Nature **178**, 1046 (1956); G. Goldhaber *et al.*, Phys. Rev. **120**, 300 (1960); P. L. Jain, W. M. Labuda, Z. Alimad and G. Pappas, Phys. Rev. D **8**, 7 (1973).

[4] W. R. Frazer *et al.*, Rev. Mod. Phys. **44**, 284 (1972).

[5] G. I. Kopylov and M. I. Podgoertsky, Yad Fiz. **15**, 392 (1972) [Sov. J. Nucl. Phys. **15**, 219 (1972)]; **19**, 434 (1974) [**19**, 215 (1974)]; G. I. Kopylov, Phys. Lett. B **50**, 572 (1974).

[6] F. Cooper, R. C. Hwa and I. Sarcevic, *Intermittenacy in High Energy Collisions* (World Scientific, Singapore, 1991).

[7] G. Singh, K. Sengupta and P. L. Jain, Phys. Rev. C **41**, 999 (1990); P. L. Jain, K. Sengupta, G. Singh and A. Z. M. Ismail, Phys. Lett. B **235**, 351 (1990); P. L. Jain, K. Sengupta and G. Singh, Phys. Rev. Lett. **59**, 2531 (1987); G. Singh, K. Sengupta and P. L. Jain, Phys. Rev. Lett., **61**, 1073 (1988); P. L. Jain, K. Sengupta and G. Singh, Phys. Lett. B **187**, 175 (1987).

[8] G. Singh and P. L. Jain, Z. Phys. A **348**, 99 (1994); P. L. Jain, G. Singh and A. Mukhopadhyay, Phys. Rev. C **50**, 1085 (1994); P. L. Jain and G. Singh, Phys. Rev. C **49**, 3320 (1994); G. Singh and P. L. Jain, Phys. Rev. C **50**, 2508 (1994).

[9] P. L. Jain, K. Sengupta and G. Singh, Phys. Rev. C **44**, 844 (1991).

[10] P. L. Jain and G. Das, Phys. Rev. D **23**, 2506 (1981); G. M. Chernov *et al.*, Nucl. Phys. A **280**, 478 (1977); G. Baroni *et al.*, Nucl. Phys. B **103**, 213 (1976); L. Foa, Phys. Rep. **22**, 1 (1975).

[11] W. Bell *et al.*, Z. Phys. C **22**, 109 (1984).

[12] P. L. Jain and G. Singh, Mod. Phys. Lett. A **9**, 1445 (1994).

Figure Captions

Fig. 1 (a) The normalized two-particle correlation functions $R_2(\eta_1, \eta_2)$ at equal pseudorapidities, as a function of η for: (i) ^{197}Au ion at 10.6A GeV (closed circles) and (ii) ^{28}Si beam at 14.5A GeV (open circles). (b) Same as Fig. 1(a), but for: (i) ^{32}S ion at 200A GeV (open squares), (ii) ^{16}O beam at 200A GeV (filled triangles) and (iii) ^{16}O projectile at 60A GeV (open triangles).

Fig. 2 $R_2(\eta_1, \eta_2)$ as a function of η at equal pseudorapidities in three intervals of shower-particle multiplicity: for the ^{197}Au data at 10.6A GeV (a) $N_s \leq 150$, (b) $150 < N_s \leq 250$ and (c) $N_s > 250$; for the ^{32}S data at 200A GeV (d) $N_s \leq 150$, (e) $150 < N_s \leq 250$ and (f) $N_s > 250$.

Fig. 3 (a) The normalized three-particle correlation functions $R_3(\eta_1, \eta_2, \eta_3)$ at $\eta_1 = \eta_2 = \eta_3$, as a function of η for: (i) ^{197}Au ion at 10.6A GeV (closed circles) and (ii) ^{28}Si beam at 14.5A GeV (open circles). (b) Same as Fig. 3(a), but for: (i) ^{32}S beam at 200A GeV (open squares), (ii) ^{16}O ion at 200A GeV (filled triangles) and (iii) ^{16}O nucleus at 60A GeV (open triangles).

Fig. 4 The normalized three-particle correlation functions $R_3(\eta_1, \eta_2, \eta_3)$ against η with $\eta_1 = \eta_2 = \eta_3$ in three intervals of shower-particle multiplicity: for the ^{197}Au data at 10.6A GeV (a) $N_s \leq 150$, (b) $150 < N_s \leq 250$ and (c) $N_s > 250$; for the ^{32}S data at 200A GeV (d) $N_s \leq 150$, (e) $150 < N_s \leq 250$ and (f) $N_s > 250$.

Fig. 5 (a) The normalized two-particle correlation functions $R_2(\phi_1, \phi_2)$ at equal azimuthal angles $\phi_1 = \phi_2$, as a function of ϕ (deg) for: (i) ^{197}Au ion at 10.6A GeV (closed circles) and (ii) ^{28}Si beam at 14.5A GeV (open circles). (b) Same as Fig. 5(a), but for: (i) ^{32}S ion at 200A GeV (open squares), (ii) ^{16}O ion at 200A GeV (filled triangles) and (iii) ^{16}O ion at 60A GeV (open triangles).

Fig. 6 The normalized two-particle correlation functions $R_2(\phi_1, \phi_2)$ at $\phi_1 = \phi_2$, as a function of ϕ (deg) for the most central events with $N_s > 250$ of: (i) ^{197}Au ion at 10.6A GeV (closed circles) and (ii) ^{32}S beam at 200A GeV (open squares). Errors plotted in this figure are of statistical nature.

Fig. 7 (a) The normalized three-particle correlation functions $R_3(\phi_1, \phi_2, \phi_3)$ at $\phi_1 =$

Fig. 3 ⇒

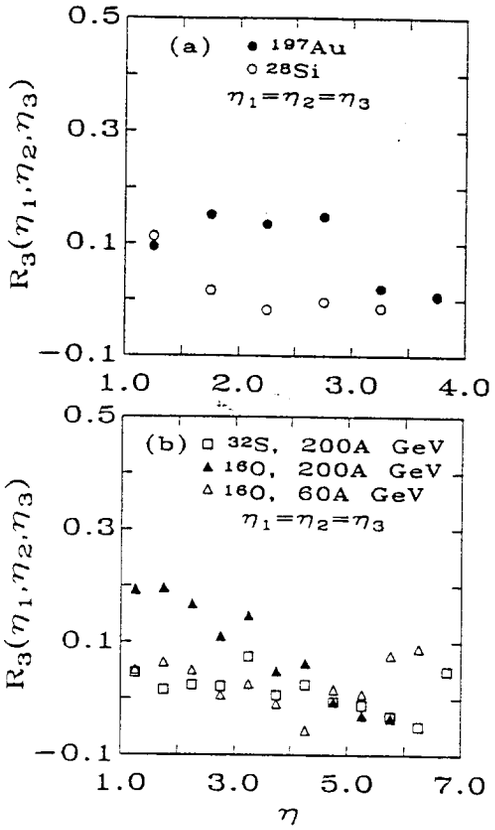

$\phi_2 = \phi_3$, as a function of ϕ (deg) for: (i) ^{197}Au beam ion at 10.6A GeV (closed circles) and (ii) ^{28}Si ion at 14.5A GeV (open circles). (b) Same as Fig. 6(a), but for: (i) ^{32}S beam at 200A GeV (open squares), (ii) ^{16}O ion at 200A GeV (filled triangles) and (iii) ^{16}O projectile at 60A GeV (open triangles).

Fig. 8 The normalized three-particle correlation functions $R_3(\phi_1, \phi_2, \phi_3)$ at $\phi_1 = \phi_2 = \phi_3$, as a function of ϕ (deg) for the central events with $N_s > 250$ of: (i) ^{197}Au ion at 10.6A GeV (closed circles) and (i) ^{32}S beam at 200A GeV (open squares). Errors plotted in this figure are of statistical nature.

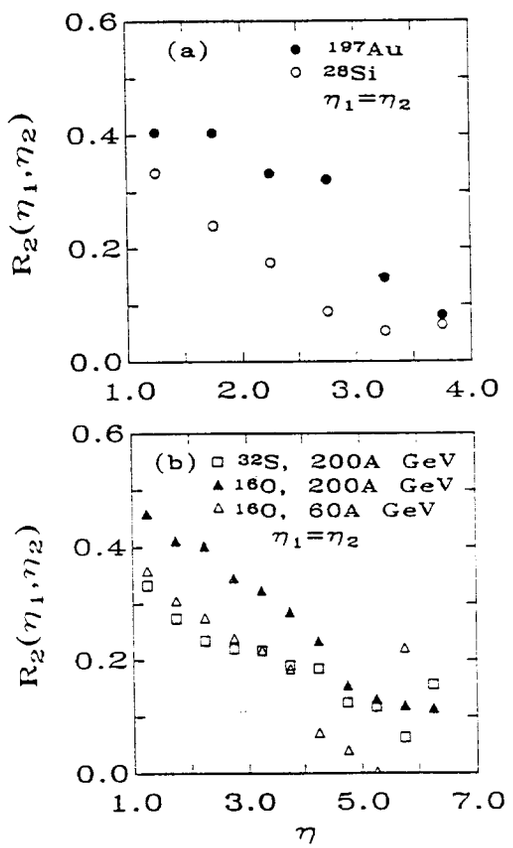

Muhhopadhyay et al. Fig. 1

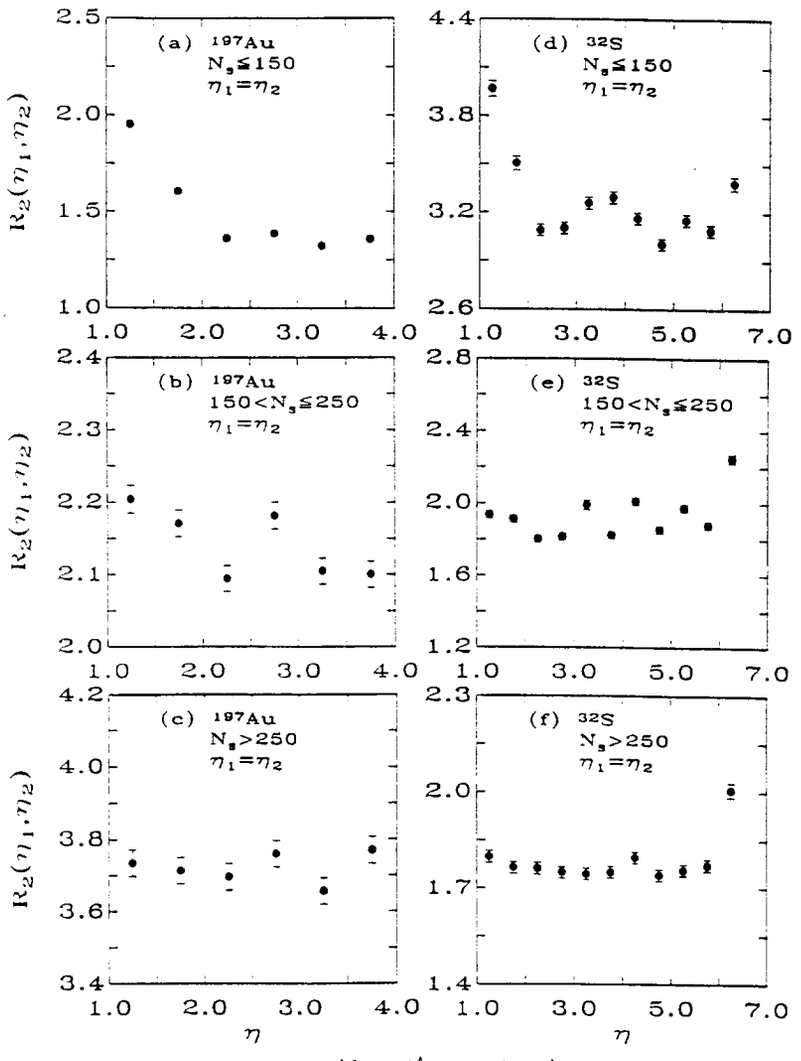

Muhhopadhyay et al. Fig. 2

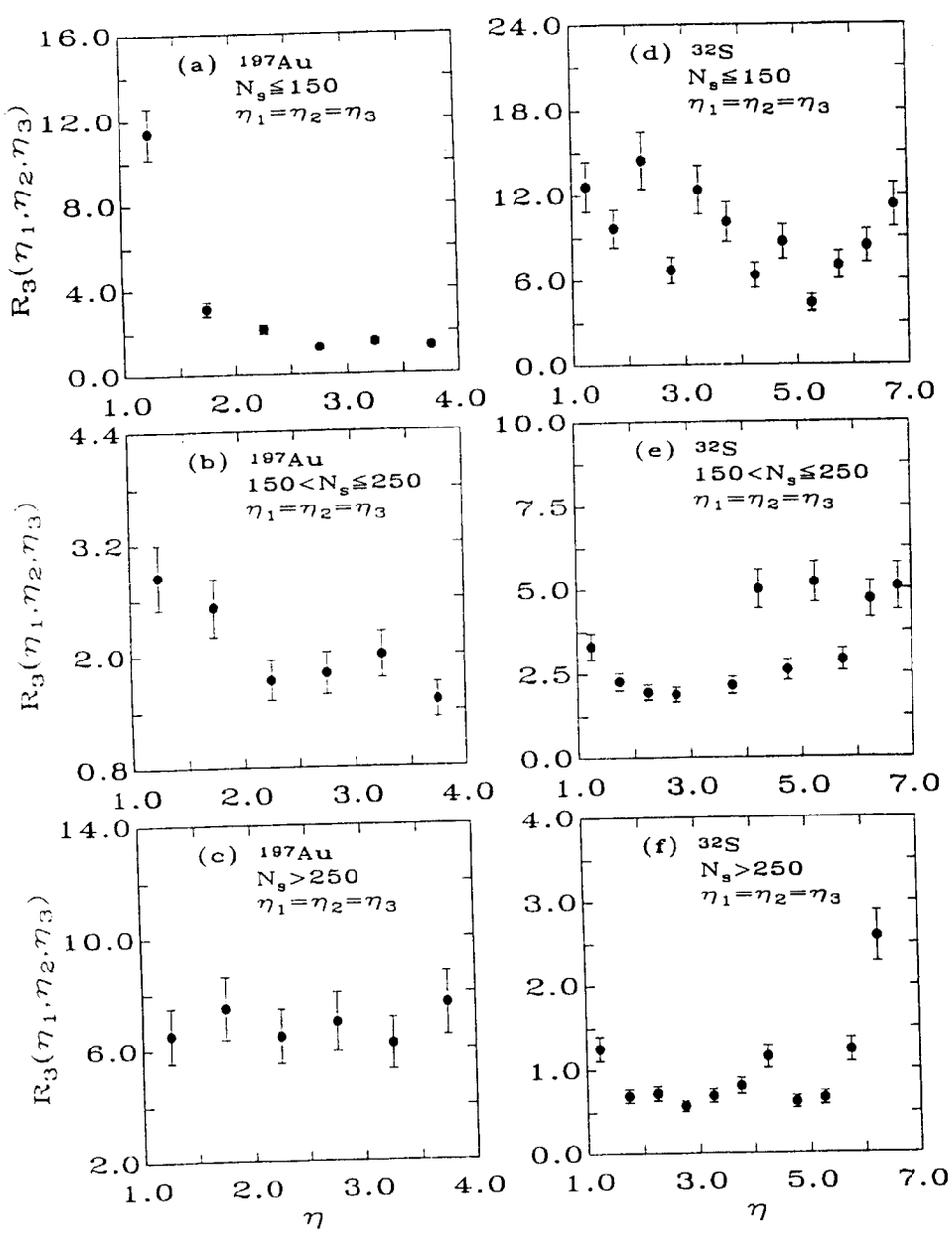

Mukhopadhyay et al. Fig. 4

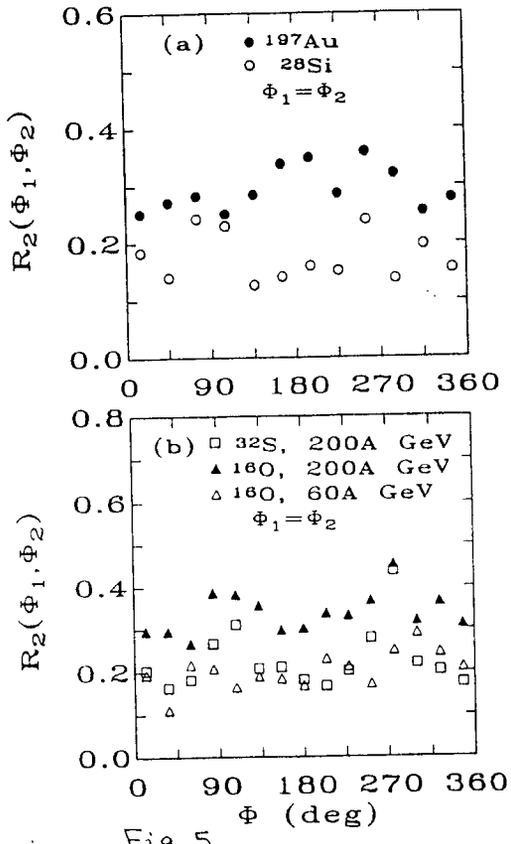

Fig. 5

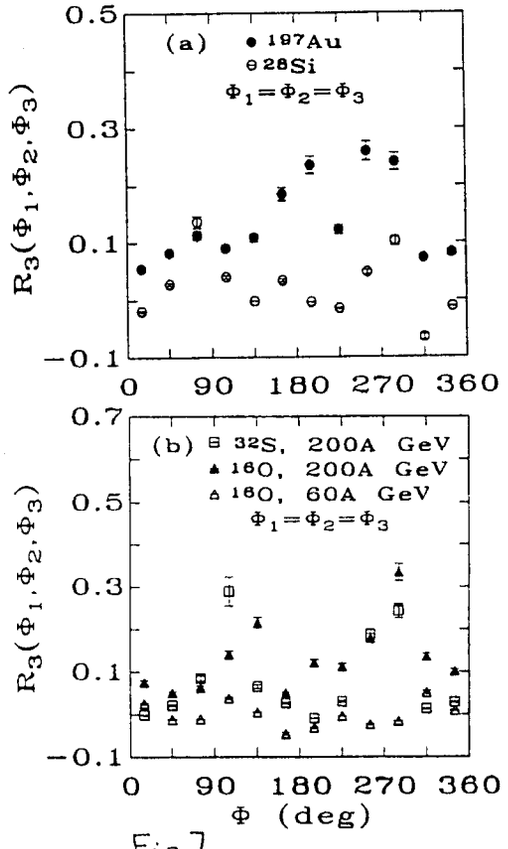

Fig 7

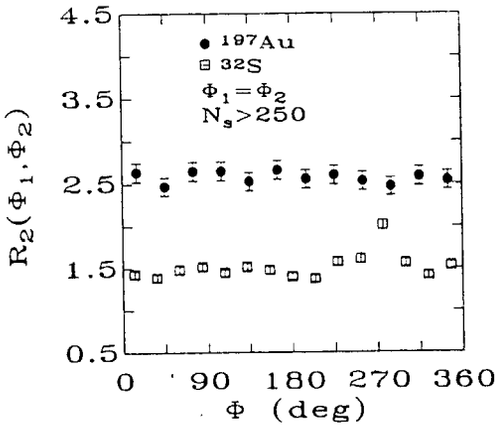

Fig. 6

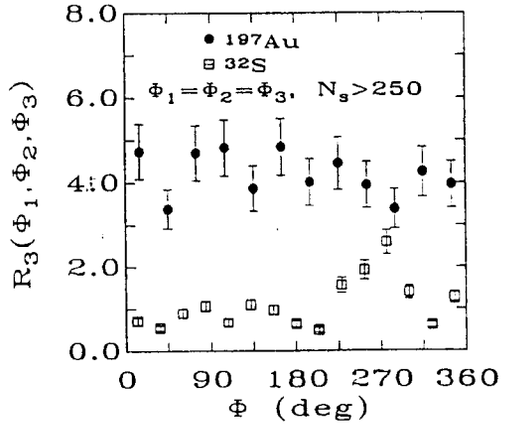

Fig. 8